Nanoscale

Nanoscale

ARTICLE

Engineering of supramolecular photoactive protein architectures: Defined co-assembly of photosystem I and cytochrome *c* using a nanoscaled DNA-matrix

Kai R. Stieger*[a], Dmitri Ciornii[a], Adrian Kölsch[b], Mahdi Hejazi[b], Heiko Lokstein[c], Sven C. Feifel[a], Athina Zouni[b] and Fred Lisdat*[a]

The engineering of renewable and sustainable protein-based light-to-energy converting systems is an emerging field of research. Here, we report on the development of supramolecular light-harvesting electrodes, consisting of the redox protein cytochrome c working as a molecular scaffold as well as a conductive wiring network and photosystem I as a photo-functional matrix element. Both proteins form complexes in solution, which in turn can be adsorbed on thiol-modified gold electrodes through a self-assembly mechanism. To overcome the limited stability of self-grown assemblies, DNA, a natural polyelectrolyte, is used as a further building block for the construction of a photo-active 3D architecture. DNA acts as a structural matrix element holding larger protein amounts and thus remarkably improving the maximum photocurrent and electrode stability. Investigating the photophysical properties, this system demonstrates that effective electron pathways have been created.

Introduction

Engineering advanced electrode surfaces by incorporation of biomolecules is a promising and emerging field of current state-of-the-art research. The defined assembly of specific biomolecules onto such surfaces allows the adjustment of the properties of these electrodes for a desired purpose. In different applications, they can be used as biohybrid electrodes in biosensing[1,2] or for the enzyme-based synthesis of chemicals[3]. Furthermore bio-based electrical power generation is gained, when such bioelectrodes are used in bio-fuel cells[4] or photovoltaic devices.[5–9] The construction of new functional systems applying defined biomolecular arrangements leads to a deeper understanding of the molecular interactions and the conditions influencing them. In addition a trend can be seen in the development of coupling strategies, which are of more general character and not only suited for a specialized system.

Learning from nature, the utilization of light-to-charge carrier converting proteins from oxygenic photosynthesis of plants and cyanobacteria becomes more and more successful and the construction of new biohybrid solar energy-converting devices has been started.[10] In natural systems one of the light-converting "enzymes" is photosystem I (PSI).[10,11] In the thermophilic cyanobacterium *Thermosynechococcus elongatus* (*T. elongatus*) PSI is a trimeric pigment-protein super-complex, consisting of 12 different protein subunits, harboring 96 chlorophylls *a* (Chl *a*) – per monomeric subunit. Most Chls serve as light-harvesting antenna pigments and 6 Chls form an electron transport chain.[12] In PSI charge separation occurs at the luminal pigment dimer, Chl *a*/Chl *a'* (P700) finally leading to a reduction of the stromally-located terminal iron-sulfur-cluster (F_B).[11,13,14] Light-induced electron-hole pairs are restocked via cytochrome *c6* (cyt *c6*), which reduces P700, whereas the oxidation takes place at the F_B cluster, which is done by the redox protein ferredoxin (Fdx).[15]

In the last years, significant efforts were undertaken for the efficient coupling of PSI with electrodes using a vast number of strategies.[16] One issue to be addressed is the effective wiring of PSI to the electrode, which has been achieved by different surface design and chemistry.[17–25] For instance, molecular wiring has been accomplished by reconstitution of PSI with vitamin K1 derivatives[26], the application of cross-linked platinum-nanoparticle/PSI composites with ferredoxin[27] or linkage of pyrroloquinoline quinone to PSI.[28] The connection of PSI via different π-systems[29] on graphene has also been reported. A remarkable photocurrent density was shown by electrospray deposited PSI on nanostructured TiO_2.[30] Using the redox protein cytochrome *c* (cyt *c*) we[31] and others[32] have shown that the electrical wiring of PSI via an integrated protein matrix can be achieved.

[a] Technical University of Applied Sciences Wildau, Institute of Applied Life Sciences, Biosystems Technology, Hochschulring 1, 15745 Wildau, Germany.
[b] Humboldt-University of Berlin, Institute of Biology, Biochemistry and Structural Biology, Unter den Linden 6, 10099 Berlin, Germany.
[c] University of Glasgow, Glasgow Biomedical Research Centre, Institute for Molecular, Cell & Systems Biology, 120 University Place, Glasgow, G12 8TA, Scotland, UK., current address: Charles Unniversity in Prague, Department of Chemical Pysics and Optics, Ke Karlovu 3, 121 16 Prague, Czech Republic

Particularly, approaches for the integration of PSI beyond the two-dimensional limiting surface are of great interest, because they potentially allow the generation of higher photocurrents per geometrical electrode area. One strategy is the construction of multilayer PSI electrodes using the polyelectrolyte building block polybenzylviologen[33] or poly-aniline composite films.[34] Another PSI containing film has been shown via the integration into a cross-linked redox hydrogel using Osmium-complex containing polymers.[35–38] This leads to a higher PSI concentration beyond the 2D arrangement.[37] Another photo-functional film could be obtained by the incorporation of PSI into a Nafion matrix.[39] A more simple method to develop PSI multilayer-like structures has been achieved by vacuum-assisted deposition of PSI suspensions on gold[40], graphene[41,42], p-doped silicon[43] and others.[44] Furthermore, an oriented multilayer formation was also confirmed by subsequently deposition of platinized PSI.[45] Moreover, using agarose, the formation of a multilayer on charged hematite can be achieved.[46]

Previously PSI and cyt *c* have been subsequently adsorbed onto each other to form multilayer architectures.[31] Here we report the complex binding of cyt *c* with PSI for the first time. Based on this finding, we describe a time-controlled self-assembly process, due to the formation and adsorption of PSI:cyt *c* - complexes. In this study, we combine two strategies to develop a highly biocompatible, stable and sustainable light-to-current converting electrode by using the redox protein cyt *c*. To expand the accessible amount and stabilize the electrodes, we use DNA as a polyelectrolyte to provide a nanoscaled matrix for the PSI:cyt *c* - complexes on the electrode surface.

Here we exploit that cyt *c* binds with DNA via electrostatic interactions to form stable layered assemblies with a very large amount of electro-active protein.[47] In addition, it has been shown that other biomolecules, such as enzymes can be integrated into these architectures.[48–51] The remarkable features of DNA significantly enhance the electro-active cyt *c* amount as compared to other nanoscaled building blocks, such as sulfonated polyanilines (PASA)[52], modified gold[53] or silica nanoparticles.[54] This renders DNA an interesting candidate to be applied in photo-bioactive electrode structures. In this study, we describe the construction of such biohybrid electrodes and investigate the striking features of these systems.

Results and Discussion

Co-assembly of cyt *c* and PSI: Au-ML-[(PSI)$_x$:(cyt *c*)$_y$]

It has been found, that PSI can be adsorbed onto cyt *c* and *vice versa*, indicating a strong interaction between both biomolecules.[31] These proteins may also form a complex in solution with the opportunity to turn the interaction of cyt *c* and PSI into a time-controlled self-growing process. To verify pre-complex formation in solution, cyt *c* and PSI have been incubated together (see experimental details). The complexes have been purified afterwards via filtration to remove excess

cyt *c*. Fig. S1 shows the MALDI-TOF analysis of the purified complexes, exhibiting a clear mass signal of cyt *c*. This indicates that cyt *c* has bound to PSI and cannot be removed, even by several washing steps. The main driving force for this interaction is of electrostatic nature since the same kind of experiments in the presence of 100 mM NaCl inhibits complex formation by lowering the interaction between the proteins. This verifies the complex formation in solution and is the starting point for assembling these complexes onto surfaces. Moreover, efficient electron transfer from a modified gold electrode via cyt *c* to PSI can be shown with both proteins in solution. (see Experimental Section and Fig. S9).
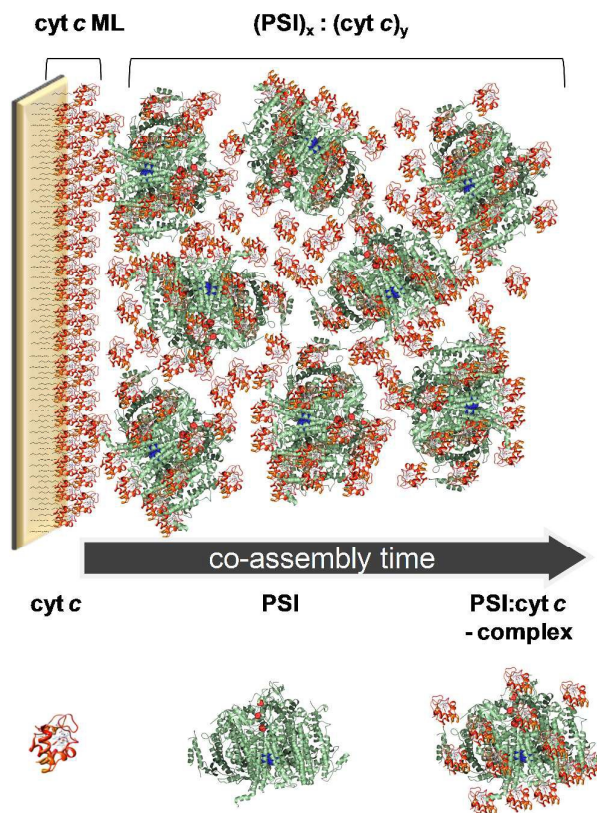
Scheme 1. Schematic representation of an Au-ML-[PSI:cyt *c*] electrode construction. The gold surface was modified with mercaptoundecanoic acid / mercaptoundecanol 1:3 (MUA/MU) adsorbing a monolayer of cyt *c* (cyt *c* ML). PSI and cyt *c* complexes were self-assembled with various molecular ratios of PSI to cyt *c* (x:y) for different time periods, allowing an increase of the photoactive protein amount on the electrode surface.

Scheme 1 illustrates the proposed concept of the co-assembly of PSI:cyt *c* complexes on an electrode. First, a cyt *c* monolayer (cyt *c* ML) is formed onto the thiol-modified gold to ensure the electrical communication of PSI with the electrode via the redox protein.[31] The heterogeneous electron transfer from the electrode towards the surface-bound cyt *c* is fast ($k_s = 70$ s^{-1}) and of quasi-reversible character providing a good basis for the subsequent electron transfer steps.

Under conditions of low ionic strength the PSI:cyt *c* complexes are found to adsorb onto a cyt *c* ML electrode and grow over time. This offers the opportunity to control the film thickness

and thus the amount of PSI on the electrode with the assembly time. The molar ratio between both proteins (PSI:cyt *c*) in the complex solution turns out to be crucial for the mass deposition and adsorption behaviour. Using a fixed assembly time the molar excess of cyt *c* has been varied from 20 to 500. In order to control the functionality of the surface assembly of both compounds photochronoamperometric measurements have been chosen. They rely on the possibility to connect PSI effectively with electrodes via the electron donor cyt *c* and exhibit a nearly exclusive cathodic photocurrent.[31]

Table 1. Photocurrent density achieved after 20 h of protein assembly onto an Au/MU:MUA/cyt *c* (cyt *c* ML) electrode from a mixture of PSI and cyt *c* with different molar ratios between PSI and cyt *c* (n = 3).

1:20 [$\mu A\,cm^{-2}$]	1:50 [$\mu A\,cm^{-2}$]	1:100 [$\mu A\,cm^{-2}$]	1:200 [$\mu A\,cm^{-2}$]	1:500 [$\mu A\,cm^{-2}$]
1.6 ± 0.4	3.2 ± 0.2	5.0 ± 0.9	7.4 ± 2.2	8.9 ± 0.2
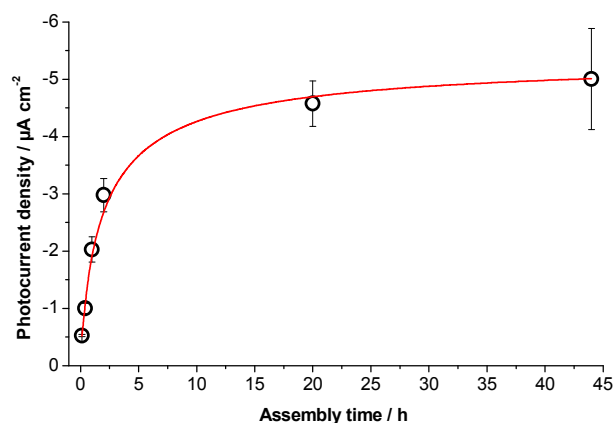
Figure 1. Photocurrent density in dependence on the assembly time. Electrodes have been modified with a cyt *c* ML, then PSI and cyt *c* have been co-assembled for different time periods from a 1:100 mixture of both proteins. Photochronoamperometric measurements have been carried out under aerobic conditions at RT in phosphate buffer (5 mM, pH 7) at a potential of -100 mV vs. Ag/AgCl using white light of 20 mW cm^{-2} (n = 4).

The functionality of electrodes prepared with different protein ratios can be seen from the data compiled in Tab. 1. The table displays major differences in photocurrent output for varying molar excesses of cyt *c* at a specific assembly time. Larger amounts of cyt *c* lead to an increase in photocurrent, which seems to level off at a 200-fold cyt *c* excess (see also Fig. S2).

Furthermore, the time dependence of the assembly of the PSI:cyt *c* complex has been studied at a fixed molar ratio (1:100) as given in Fig. 1. After a longer exposure time (44 h) a saturation of the photocurrent becomes visible. This indicates that either i) equilibrium of adsorption and desorption from/to the surface is reached during preparation, or ii) electron transfer to PSI molecules immobilized far away from the electrode surface is not sufficient anymore. Here, a hyperbolic function can be found to fit the data points giving characteristic parameters of the time-controlled co-assembly process (K_{50} = 122 ± 43 min, J_{max} = 5.4 ± 0.6 $\mu A\,cm^{-2}$, regression coefficient R^2 = 0.98).

To gain further insights in the co-assembly process, surface plasmon resonance (SPR) experiments have been carried out, elucidating the mass accumulation on the cyt *c* ML (see Fig. 2). Thus, repeated injections of the protein mixture are used to verify both the mass deposition and the adsorption kinetics of the co-assembly. Here, two different molar ratios of cyt *c* and PSI have been tested, which have resulted in a significantly different photocurrent density: 1:100 (5 ± 0.9 $\mu A\,cm^{-2}$) and 1:20 (1.6 ± 0.4 $\mu A\,cm^{-2}$). For the experiment 6 subsequent flushes of PSI:cyt *c* complexes over the surface with intermittent buffer flow have been performed.

For short assembly times (up to 16 min), no significant difference of mass deposition on the surface is detected. For longer exposure times the mass deposition from a solution of a molar ratio of 1:100 yields a higher mass correlated signal. For both cases a saturation behaviour is observed, however saturation for 1:20 solution starts earlier. The total amount of proteins on the surface (proportional to the SPR signal) is lower compared to the deposition from a 1:100 solution.

Via cyclic voltammetry the redox reaction of immobilized cyt *c* in the co-assembly on the gold electrode can be verified, while the transferred charge in the film corresponds to the electro-active amount of deposited cyt *c*. The redox protein can be detected within the protein architecture even when fixed further away from the electrode surface because of self exchange between the cyt *c* molecules. This property does not only result in the electrochemical addressability of many layers of cyt *c* but has also been exploited in connecting enzyme molecules in different layers with the electrode.[47,50]
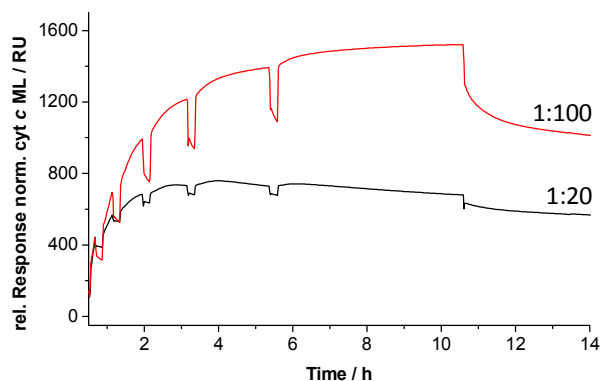
Figure 2. Surface plasmon resonance (SPR) sensorgram of the co-assembly of PSI:cyt *c* complexes on modified gold surfaces. All experiments have been performed in phosphate buffer (5 mM, pH 7) at RT in a flow system (1 mL min^{-1}). A mixture of 11-mercaptoundecanoic acid (MUA) and 11-mercapto-1-undecanol (MU) (1:3) has been used for SAM formation on the gold surface prior to the protein assembly. First, a cyt *c* monolayer (cyt *c* ML) was formed on the surface by flushing cyt *c* (30 μM, 1 mL min^{-1}) over the surface (not shown). Afterwards a pre-mixed solution of PSI:cyt c (1:100 – red curve, 1:20 – black curve) was injected for 8, 16, 36, 60, 120 and 300 min, respectively with intermittent buffer flushes. The SPR signal has been normalized to the mass signal of the cyt *c* ML.
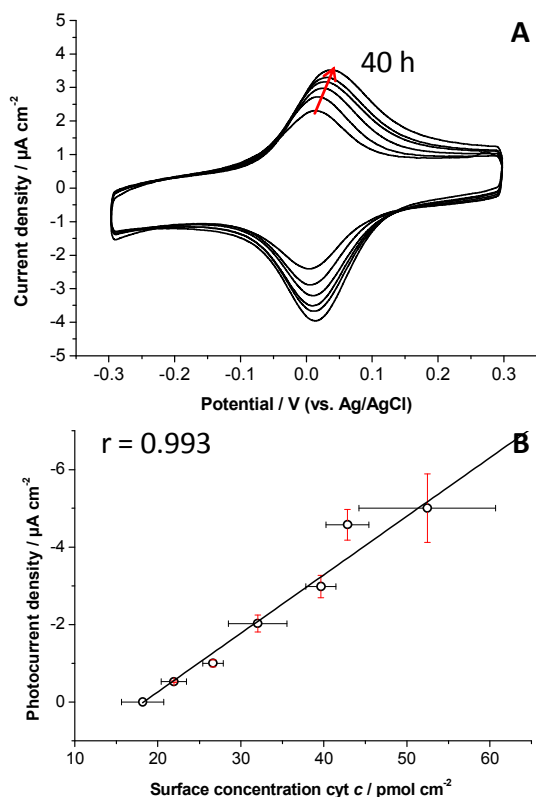
Figure 3. (A) Cyclic voltammetry of Au-ML-(PSI:cyt *c*) electrodes for different assembly times (0, 8, 24, 60, 120 min, 20 and 40 h) in phosphate buffer (5 mM, pH 7) at RT using a scan rate of 100 mV s^{-1}. The red arrow indicates the increase in peak current with the incubation time. **(B)** Correlation plot of photocurrent density against electro active surface concentration of cyt *c*, determined via cyclic voltammetry (Pearson's correlation coefficient r = 0.993, n = 4).

In Fig. 3A the increase in peak current and thus the transferred charge from/to cyt *c* within the PSI:cyt *c* assemblies can be followed with the incubation time of the electrode in the protein mixture. Additionally, there is a slight increase in peak separation (from 15 mV to 22 mV) so as half peak width (from 92 ± 8 mV to 144 ± 11 mV) with raising assembly times. This indicates that with increasing protein mass on the surface the electron transfer through the assembly is slowing down. Furthermore, the heterogeneity of the cyt *c* micro-environment rises. For electrodes, which have been obtained after different assembly times, the cyt *c* surface concentration can be plotted against the generated photocurrent density. A correlation between the electro-active cyt *c* amount and the functional PSI - indicated by the photocurrent - is received (Fig. 3B, Pearson's correlation coefficient r = 0.993). This corresponds to the idea of well connected PSI molecules within the 3D architecture and reveals that both proteins assemble jointly to the surface.

Taken together, a higher molar excess of cyt *c* to PSI results not only in a faster adsorption on the electrode, but displays an increase in photocurrent. Within these architectures the cyt *c*–cyt *c* electron self-exchange, which is necessary for the reduction of PSI, is not the limiting parameter. Even PSI molecules far away from the electrode surface can still be

electrically addressed, which improves the efficiency compared to a 2D photo-reactive electrode design.[31]

The equilibrium condition at which the rate of adsorption equals the rate of desorption can be tuned by the molecular excess of cyt *c*. We conclude, that cyt *c* by itself plays a major role for the structural integrity of the deposited film. Hence, in addition to its function to create electron pathways within the structure, cyt *c* acts as molecular scaffold between the PSI molecules and may also stabilizes the large membrane protein in detergent-diminished solution.

Multilayer electrodes: Au-ML/DNA-[PSI:cyt *c*/DNA]$_n$

To address the limiting features of the co-assembly PSI:cyt *c* electrode with respect to the structural thickness and stability, the assembly strategy has been further improved. Therefore, the idea of stabilizing the assembly via a further building block is applied to extend the photoactive and connected protein amount on the surface. Here, the natural biopolymer DNA from *calf thymus* is used to increase the cohesion of the photoactive protein arrangement mainly because of the strong interaction of cyt *c* and DNA (see scheme 2).
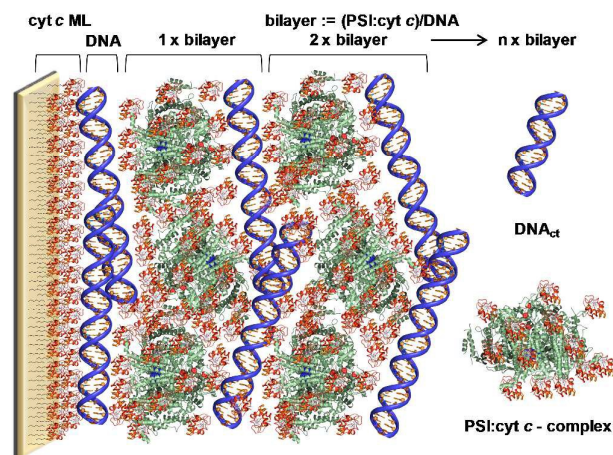
Scheme 2. Schematic representation of the construction of Au-ML-DNA-[PSI:cyt *c*/DNA]$_n$ electrodes. The gold surface is modified with mercaptoundecanoic acid / mercaptoundecanol 1:3 (MUA/MU) adsorbing a monolayer of cyt *c* (cyt *c* ML). Successive assembly of DNA and PSI:cyt *c* complexes (bilayer) is performed by the layer-by-layer technique for the construction of a photo-functional biomolecular multilayer electrode. Three different matrix elements are used here, cyt *c* – conductive element, PSI – photo-sensitive element, DNA – structural element.

Cyt *c* binds electrostatically with mainly positively charged residues to the backbone of DNA, having the strongest complex formation between both biomolecules in a low ionic strength buffer at pH 5. The biomolecular interaction has been studied previously[55] and shown to allow a high mass deposition of the redox protein on surfaces. Additionally, it has been verified that DNA does not hinder cyt *c*-cyt *c* electron transfer and thus allows the preparation of protein multilayer electrodes with a rather high amount of redox-active cyt *c*.[47]

These properties are exploited here for the construction of PSI electrodes. Basically the layer-by-layer technique is used to alternately deposit DNA and PSI:cyt *c* complexes for a specific time, to build up multilayered PSI:cyt *c*/DNA biocomposites. A

simultaneous adsorption of these three molecules from solution is not suitable, since for the deposition of DNA on cyt *c* low ionic strength and pH 5 have to be used.[47] In such a layered surface structure each biological building block has its own unique function: DNA acts as stabilizing matrix and scaffold, cyt *c* as electron shuttle and assembly template for PSI and PSI as a photo-functional building block.

SPR measurements show an alternating deposition of DNA on top of the PSI:cyt *c* surface, as *vice versa* (Fig. S5). An assembled PSI:cyt *c* structure with DNA exhibits a ~1.6 fold increased mass deposition on the surface under the same experimental conditions compared to a control without DNA (both prepared with 6 deposition steps).
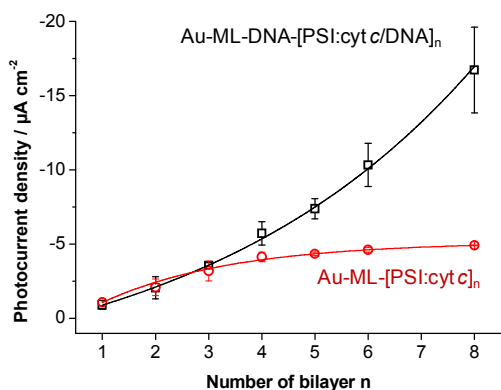
Figure 4. Dependence of the photocurrent density on the number of deposition steps *n* of the DNA-electrode (Au-ML-DNA-[PSI:cyt *c*/DNA]$_n$, black) and the co-assembly electrode (Au-ML-[PSI:cyt *c*]$_n$, red). Photochronomperometric measurements have been carried out under aerobic conditions at RT in phosphate buffer (5 mM, pH 7) at a potential of -100 mV vs. Ag/AgCl using white light of 20 mW cm^{-2} (n = 4).

In Fig. 4 a comparison of photocurrent densities of DNA-based electrodes (Au-ML-[PSI:cyt *c*/DNA]$_n$) and electrodes prepared by simple co-assembly of PSI:cyt *c* (Au-ML-[PSI:cyt *c*]$_n$) for a different number of deposition steps is shown. Since there is no second building block for the co-assembly electrode, the electrode was prepared from a PSI:cyt *c* solution maintaining the same incubation times as for the DNA-based electrode to guarantee a better comparability. Until three incubation steps in the PSI:cyt *c* solution there is no significant difference found between the construction of the electrode with or without DNA. After the 4th assembly step a saturation of photocurrent density is observed with the co-assembly electrodes (as already mentioned in the first section). The generated photocurrent of the DNA-based electrode increases exponentially and no saturation is found up to the 8th bilayer. The DNA-based electrodes circumvents the limiting issue of the co-assembly electrode by allowing further protein deposition followed by a strong rise in photocurrent output.

By investigating the PSI:cyt *c*/DNA systems by means of cyclic voltammetry a clear cyt *c* signal has been obtained (see Fig. 5A).
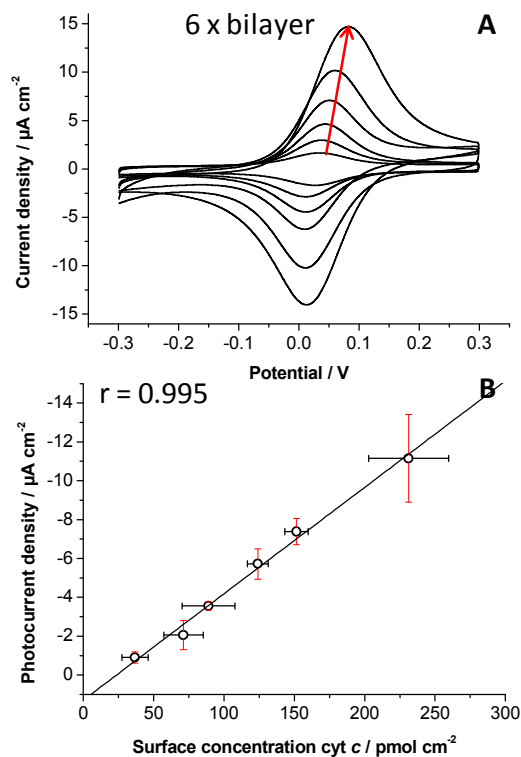
Figure 5. (A) Cyclic voltammograms of Au-ML-DNA-[PSI:cyt *c*/DNA]$_n$ electrodes with different bilayers (1x-6x) in phosphate buffer (5 mM, pH 7) at RT using a scan rate of 100 mV s^{-1}. The red arrow indicates the increase in peak current with the bilayer number. The potential is given vs. Ag/AgCl, 3 M KCl. **(B)** Correlation plot of photocurrent density obtained with Au-ML-DNA-[PSI:cyt *c*/DNA]$_n$ electrodes against the electro-active cyt *c* concentration of these electrodes determined via cyclic voltammetry (Pearson's correlation coefficient r = 0.995, n = 4).

With each bilayer the peak current and thus the transferred charge increases. A high electro-active surface concentration of cyt *c* is found for 6x bilayer (231 ± 28 pmol cm^{-2}, n = 4). Furthermore, the DNA-based electrode exhibits a quasi-reversible electron transfer with a formal potential of 39 ± 5 mV vs. Ag/AgCl and a peak current ratio (I_{pox}/I_{pred}) of ~1 for different numbers of bilayers. The half peak width changed from 92 ± 8 mV for a cyt *c* ML (n = 5) to 140 ± 3 mV for a 6x bilayer (n = 5). These results can be explained by the different microenvironment of bound cyt *c* in the multilayer assembly with the large membrane protein PSI. The resulting distribution of redox states and orientation of the cyt *c* heme exhibits a broadening in redox peaks.

The peak separation also increases with the number of bilayers (Fig. S3) from 13 ± 4 mV (cyt *c* ML, n = 5) to 66 ± 9 mV (6x bilayer, n = 5), thus the electron transfer kinetics is more and more influenced by the electron transport between the assembled cyt *c* molecules. If the resulting photocurrent density of each electrode is plotted against the surface concentration of cyt *c* (which was obtained via cyclic voltammetry), a good correlation can be seen (Fig. 5B, Pearson's correlation coefficient r = 0.995). This indicates that

also with the newly developed assembly strategy both proteins adsorb as a complex from the solution to the surface. In comparison to the co-assembly electrode, the increase in photocurrent is due to a higher amount of assembled proteins. If cyt c is left out during the assembly process, only minor non-directional photocurrents are achieved, showing that DNA does not take part in die electron transfer and cyt c is needed for the connection of the PSI molecules in the different layers (see Fig. S6). This also seems to be reasonable considering the redox potential of G-bases in DNA (0.81 V vs. NHE)[56] and the potential of P700 (0.43 V vs. NHE)[57]. Furthermore the photoaction spectrum of this system demonstrates that the photocurrent follows the absorption spectrum of PSI in solution, and also the absorption of a 6x bilayer assembly, and therefore originates from the photoexcitation of PSI (Fig. S10).

At least for the tested assembly numbers of PSI:cyt c/DNA, the photocurrent correlates with the PSI concentration, thus verifying that cyt c self exchange within the architecture can provide the necessary electrons for PSI reduction even when PSI is located far away from the electrode surface. A second result is the feature of DNA, which does not alter the working properties of the co-assembly, acting only as a structural framework without any electrochemical activity within this potential range. This overcomes the limitation of the co-assembly method and extends the electrode structure towards a larger photo-functional film thickness.

Features of the Au-ML-[PSI:cyt c/DNA]$_n$ electrode

One of the indicated features of DNA-based assemblies is the surface enlargement during the deposition of multiple layers. Scanning electron microscopy images have been displayed to verify this claim (see Fig. 6).
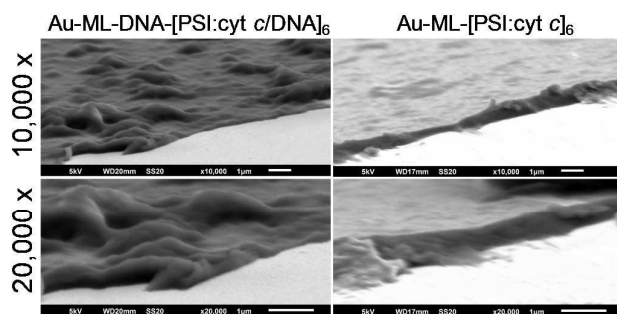
Figure 6. Scanning electron microscopy (SEM) images of 6 bilayer assemblies prepared in the presence or absence of DNA: Au-ML-DNA-[PSI:cyt c/DNA]$_6$ and Au-ML-[PSI:cyt c]$_6$. A magnification of 10,000x, 20,000x and a voltage of 5 kV were used. White bars indicate the scale (1 μm).

A rather high surface roughness can be seen for the DNA-based electrode compared to the co-assembly electrode. Here, the DNA-based PSI:cyt c assemblies form films of different height (250 – 700 nm) with additional islands. On the contrary, the PSI:cyt c co-assembly form a rather flat and smooth film. The height of this deposition is much more uniform and around 500 nm. The comparatively rough surface of the DNA-based electrodes indicates an increased overall biomolecule

mass on the surface and correlates well with the higher photocurrent densities found for this system.

This is also in very good agreement with the photocurrent differences found between the electrodes. The output of the DNA-electrode is for 6x bilayers twice as high as for the co-assembly electrode with the same number of assembly steps (see Fig. 4). Since, there is no additional photoactive element used in the DNA-assembly, the overall output corresponds only to the amount of connected PSI on the surface. While DNA could also disturb the connection between cyt c and PSI, and lower the active amount of PSI, the relatively good correlation between the surface structure and the photocurrent contradicts to this assumption.

In this section we also provide insight into the photoelectrochemical properties of the DNA-based electrode. For the photocurrent densities it has to be mentioned that no additional electron acceptor has been used in the solution so far. Under such conditions electrons from the reduced F_B^- ($E^{0'}$ = -0.53 vs. NHE[58]) can be transferred to molecular oxygen. A high photocurrent density with only oxygen in the solution can be obtained with 8x bilayers (17 ± 3 μA cm^{-2}, n = 3). In order to elucidate the limiting step of the electron transfer cascade methyl viologen (MV^{2+}) has been used as an additional electron acceptor for F_B^- (in addition to the presence of molecular oxygen). This approach in testing photocatalytic systems with MV^{2+} has been used previously, since it was reported that the presence of MV^{2+} can enhance the electron withdrawal from photo-excited PSI.[59,60] A recent study has proposed that this is probably caused by a first reaction of oxygen with MV^{2+}, which then oxidizes the reduced F_B cluster of PSI.[61]
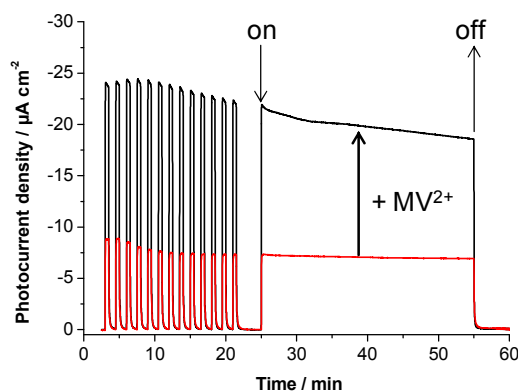
Figure 7. Photochronoamperometric measurement of an Au-ML-DNA-[PSI:cyt c/DNA]$_6$ electrode (6x bilayer) at RT in phosphate buffer (5 mM, pH 7) with 1 mM MV^{2+} (black) and without (red). A 20 mW cm^{-2} light intensity (white light) was used for light pulses of 15 s and for a longer exposure time of 30 min. The potential was fixed at -100 mV vs. Ag/AgCl.

This would also agree with our experiments since in the absence of oxygen, MV^{2+} additions have no effect on the photocurrent. By the addition of MV^{2+} one can test whether the photobiohybrid system is limited by electron transfer to the excited PSI or electron withdrawal from PSI. Consequently, the influence of MV^{2+} in solution on the photocurrent has been

evaluated with a 6x bilayer electrode. A remarkable photocurrent density increase can be obtained by adding MV^{2+}, here the current becomes a factor of 2.7 higher (increase from ~9 to ~24 µA cm^{-2}).

This verifies that the overall electron transfer process in the system is not mainly limited by cyt *c*, but by electron withdrawal from the excited PSI. The photo-induced cathodic electron transfer for these electrodes starts at about 60 mV vs. Ag/AgCl, which can be seen from voltammetric experiments with and without illumination of the surface (see Fig. S4). Here, the onset of photocurrent is mainly determined by the redox properties of cyt *c*, which demonstrates the wiring properties of the redox protein, i.e. cyt *c* needs to be reduced before electrons can be transferred to PSI. This is in agreement with previously reported findings[31]. No anodic catalysis has been found verifying the photodiode character of the protein architecture.
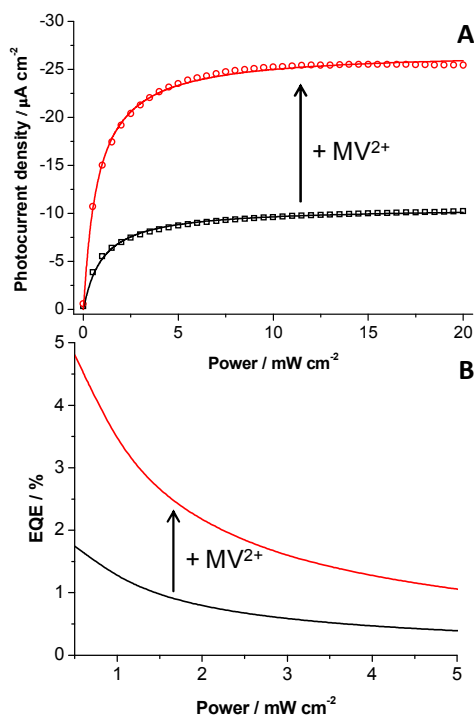
Figure 8. (A) Dependence of the photocurrent density of an Au-ML-DNA-[PSI:cyt *c*/DNA]$_6$ electrode on the light intensity with (red) and without (black) MV^{2+}. Experiments have been performed under aerobic conditions at RT in phosphate buffer (5 mM, pH 7). Data were fitted with the Michaelis-Menten equation. Parameters have been elucidated with MV^{2+} (K_M = 0.77 ± 0.02 mW cm^{-2}, I_{max} = 26.8 ± 0.1 µA cm^{-2}, regression coefficient R^2 = 0.994) and without (K_M = 1 ± 0.02 mW cm^{-2}, I_{max} = 10.6 ± 0.1 µA cm^{-2}, regression coefficient R^2 = 0.994). **(B)** Calculated external quantum efficiency (EQE) of an Au-ML-DNA-[PSI:cyt *c*/DNA]$_6$ electrode as a function of light intensity with (red) and without (black) MV^{2+}.

The proposed mechanism of electron transfer in the assembly starts at the electrode where cyt *c* is reduced and is followed by subsequent interprotein electron transfer steps between the cyt *c* molecules and cyt *c* to PSI finally resulting in electron transfer from PSI to oxygen (or oxygen+MV^{2+}). This is schematically shown in the supporting information (Fig. S11).

Another interesting feature of these electrodes is the photocurrent stability, which is shown in Fig. 7. After several times of 30 s light exposure, the electrode exhibits a rather stable photocurrent. When illuminated for 30 min with constant light (power of 20 mW cm^{-2}) a moderate photocurrent decrease of about 16 % is observed using MV^{2+} in solution. On the contrary the reduction of photocurrent without MV^{2+} by exposing the electrode to light is very small (~3 %). This finding might be explained by a rather fast depletion of MV^{2+} near the electrode surface. Nevertheless, remarkable photocurrent stability has been found, additionally underpinning the pronounced stability of the protein-DNA framework. Ancillary, long term storage experiments have been performed. Storing the electrodes in buffer solution results in a reduction of photocurrent within the time frame of several days. Cyclic voltammetric experiments suggest that the framework tends to lose connection with the electrode (data not shown).

However, when the electrodes are stored dry at 4 °C after 9 d of storage the DNA-based electrodes exhibit still 94 ± 13 % (n = 3) of its starting activity, which is in comparison to the co-assembly electrode much more stable (only 25 ± 10 %, n = 3). Even after 1 month of storage ~65 % of the activity is retained with the DNA-electrode (see Fig. S7). This is remarkable particularly since the electrodes have been measured several times during the storage period. The usability of the electrode over a longer time period provides the next advantageous feature of the system.

In the following set of experiments the dependency of the photocurrent density on the light power has been investigated (see Fig. 8A). Considering photons as the substrate for a photo-reactive enzyme such as PSI, the Michaelis-Menten equation can be used to fit the experimental data, which was proposed previously.[29,31,35] As there is no additional photon-to-current converting species in the system, the cooperativity *n* was chosen to be 1. The parameters of K_M and v_{max} can be calculated for a 6x bilayer electrode (K_M = 1 ± 0.02 mW cm^{-2}, J_{max} = 10.6 ± 0.1 µA cm^{-2}, regression coefficient R^2 = 0.994). When using MV^{2+} as an additional electron acceptor in solution, the overall photocurrent density increases significantly (J_{max} = 26.8 ± 0.1 µA cm^{-2}, regression coefficient R^2 = 0.994), as already mentioned (see Fig 7). The light power at the half-maximum of photocurrent undergoes a slight decrease (K_M = 0.77 ± 0.02 mW cm^{-2}). This result points out, that without MV^{2+} the withdrawal of electrons from the F_B is the rate limiting step of electron flow in the system, because of either low electron acceptor concentration in solution or slow electron transfer rate of the oxidation of F_B with oxygen. This behaviour changes after the addition of MV^{2+}. Under these conditions the light-to-current conversion of the PSI multilayer electrode seems to be limited by the electron transfer of the electron shuttle to PSI. This can be concluded considering the fast intramolecular rate of charge separation (~1 µs) upon PSI illumination and a quantum yield of PSI of nearly 100 %.[11,62] The lower K_M value after the addition of MV^{2+} indicates, that the efficiency of light conversion is improved by the additional electron acceptor in this system.

Proux-Delrouyre *et al.* have also shown, that at a high molecular excess of MV^{2+} with respect to the natural electron donor cyt c_6 the apparent rate constant reaches the rate constant of P700 reduction by cyt c_6 and thus the latter process becomes the rate limiting step.[63] PSI concentration has been determined for a 6x bilayer electrode following chlorophyll extraction. The total density of PSI in this assembly is 13 ± 2 pmol cm^{-2} (n = 3). With MV^{2+} in solution a turnover number of 21 ± 2 s^{-1} can be calculated.

For the usage in a photovoltaic setup, the external quantum efficiency (EQE) can be estimated, which is defined as the ratio of the collected number of carriers (n_e) to the number of incident photons (n_p) at a given energy:

$$EQE = \frac{n_e}{n_p}.$$

In Fig. 8B the EQE is calculated and plotted against the light power used for excitation. Here, for all light intensities an overall higher quantum efficiency can be obtained, when MV^{2+} is used. At light intensities of half maximum (0.77 mW cm^{-2}) a EQE of 4.1 % is achieved. This is in the same order of magnitude of values found for other 3D PSI architectures.[35] The internal quantum efficiency (IQE), considering only the absorbed photons, has also been estimated from the PSI absorption spectrum in solution corrected for the number of PSI complexes in a 6x bilayer assembly (and considering the spectral properties of the white light source used for the photocurrent measurements). At half-maximum light intensities (0.77 mW cm^{-2}) an IQE of about 24 % is achieved, which is about 6 times larger compared to the EQE.

Conclusions

This study demonstrates a feasible proof of concept for the artificial connection of biological building blocks exploiting different biomolecular features. First, we have shown that the redox protein, cyt *c*, and a solar energy converting protein, PSI are able to form complexes in solution. Second, this biomolecular interaction has been exploited for the co-assembly of both proteins on electrode surfaces. Here, cyt *c* acts as the conductive biomolecular element, building up an electrical wiring network, which embeds PSI as the photo-functional component. As for most deposition processes from solution, self-assembly on a surface is limited by the adsorption equilibrium or the available 2D area. To overcome this problem a structural matrix element, DNA, is introduced, giving the opportunity to successively enhance the functional film thickness and thus the photocurrent output, in a layer-by-layer approach. Together these building blocks form an artificial 3D architecture exhibiting several features for future applications: A rather high stability compared to other photo-biohybrid electrodes, a reasonable and tunable photocurrent, and a renewable biological interface for the incorporation of other biomolecules. Prospects of this system can be seen since the biological assembly is not restricted to one surface or electrode material, it can be used in conjunction with different kinds of electrodes; nano-, semiconductor-, transparent or

polymer-based materials. Furthermore, the biological nature of the photobiohybrid electrode allows an excellent embedment and communication with additional biomolecules of different functions. This may raise the opportunity to develop photo-enzymatic electrodes for synthesis generating simultaneously electrical energy.

Experimental Methods

Isolation of Photosystem I from *T. elongatus*

Growth of *Thermosynechococcus elongatus* BP-1 and extraction of membrane proteins from thylakoids were performed according to Kern *et al.* 2005.[64] For the purification of PSI two chromatography steps were used. The first column was packed with Toyo Pearl DEAE 650 S (GE Healthcare) and pre-equilibrated with buffer A (20 mM MES-NaOH, pH 6.0, 20 mM CaCl$_2$, 0.02 % β-DM, 5 % glycerol). After sample loading and washing the column with buffer A, PSI was separated from PSII using a linear gradient with buffer B (20 mM MES-NaOH, pH 6.0, 20 mM CaCl$_2$, 0.02 % β-DM, 5 % glycerol, 100 mM MgSO$_4$). PSI containing peak eluted at 80-90 mM MgSO$_4$ was pooled and diluted with the same volume of buffer C (5 mM MES-NaOH, pH 6.0, 0.02 % β-DM). The second column was packed with Q-SepharoseTM Fast Flow (GE Healthcare) and pre-equilibrated with buffer D (5 mM MES-NaOH, pH 6.0, 0.02 % β-DM, 60 mM MgSO$_4$). PSI Trimer was separated from remaining PSI Monomer by linear gradient with buffer E (5 mM MES-NaOH, pH 6.0, 0.02 % β-DM, 150 mM MgSO4). The PSI Trimer eluted at 150 mM MgSO$_4$. The fractions were pooled and concentrated in an Amicon stirring cell using a Biomax 100 membrane (Millipore). Finally, the PSI Trimer was crystallised by dilution with buffer C at 4 °C until a concentration of 5 mM MgSO$_4$ was reached. The crystals were collected by centrifugation (5 min, 4 °C, 4000 xg), washed with buffer C, re-solubilized by adding buffer F (5 mM MES-NaOH, pH 6.0, 30 mM MgSO$_4$) and re-crystallised as described above. For the assembling experiments the crystals were dissolved in 100 mM phosphate buffer, pH 7.0 and diluted slowly to the final buffer concentration. The photochemical activity of PSI with cyt *c* as an electron donor was measured using a Clark electrode (Hansatech). In a finale volume of 1 mL, the reaction mixture contained variable concentrations of cyt *c*, 5 mM phosphate buffer, pH 7.0, 0.05 % β-DM, 1 mM Na-ascorbate and 170 µM methyl viologen. Sample was incubated at 20 °C and saturated light (700 µmol m^{-2} s^{-1}). The reaction was started by adding of 20 nM PSI and the initial O$_2$ consumption (10 s) was measured. For the interaction of PSI with cyt *c* a catalytic rate of 20 ± 1 s^{-1} with a Michaelis-Menten constant of 23 ± 3 µM can be determined (see Fig. S9).

Complex formation of PSI with cyt *c* in solution

PSI was mixed with cyt *c* in a ratio of 1:50. The reaction mixture containing 0.8 µM PSI, 40 µM cyt *c*, 5 mM phosphate buffer, pH 7.0, 1 mM Na-ascorbate and 0.02 % β-DM (final volume = 100 µL) was incubated for 2 min and 4 °C. A second reaction mixture was performed, in which 100 mM NaCl was

added. Subsequently, the reaction mixture was applied to a Microcon YM-100 centrifugal filter (100,000 MWCO, Amicon) and centrifuged for 7 min and 4 °C to remove excess cyt *c*. The protein complex was washed 6 times with 400 µL buffer (see above) and analysed by MALDI-TOF. The determination of protein masses was carried out in linear mode using Microflex instruments (Bruker). An equal volume of 40 % acetonitrile, 0.1 % TFA in saturated sinapinic acid was mixed with protein sample in a ratio of 1:1.

Preparation of electrodes

Au-disk-electrodes (CHI) with an accessible geometrical surface of 0.0314 cm² have been briefly cleaned with abrasive paper (P1200, P2500, P3000) and subsequently cycled between -0.2 and 1.6 V (vs. Ag/AgCl) in 100 mM sulfuric acid. Au-chip-electrodes (Micrux, Spain) with an accessible geometrical surface of 0.00785 cm² have been pre-cleaned in piranha solution (1:3 H_2O_2:H_2SO_4) for 2 min. Afterwards, electrodes have been cycled between -1.5 and 1.6 V vs. Ag/AgCl in 100 mM sulfuric acid, followed by an additional cycling between -0.2 and 1.6 V in 100 mM sulfuric acid. Subsequently, both electrode types have been incubated for 48 h at RT in an ethanolic solution of a 3:1 mixture containing 11-mercapto-1-undecanol (MU, Sigma) and 11-mercaptoundecanoic acid (MUA, Sigma). Afterwards the electrodes have been incubated in 30 µM cytochrome *c* (horse heart, Sigma) in phosphate buffer (5 mM, pH 7) for 2 h forming the cytochrome *c* monolayer (cyt *c* ML), according to Ge *et al.* 2002.[65] Before starting the assembly on the surface solutions with different molecular ratios of 1:20, 1:50, 1:100, 1:200 and 1:500 PSI:cyt *c* have been prepared in 5 mM phosphate buffer, pH 7 and these mixtures were allowed to equilibrate in the dark for 30 min at RT. For the preparation of PSI:cyt *c* – co-assembly (Au-cyt *c* ML-[PSI:cyt *c*]), the electrodes have been incubated in the PSI:cyt *c* solution in the dark at RT for various time scales, and were finally ready for measurements. In DNA-based preparations the Au-cyt *c* ML electrodes have been first incubated with 0.2 mg mL^{-1} calf thymus DNA (Sigma) in 0.5 mM phosphate buffer, pH 5 for 10 min. Afterwards the electrodes have been alternately incubated in PSI:cyt *c* solution (molecular ratio 1:100) for 20 min at RT in 5 mM phosphate buffer, pH 7, followed by an incubation for 10 min in 0.2 mg mL^{-1} DNA in 0.5 mM phosphate buffer pH 5 forming the first bilayer (PSI:cyt *c*/DNA). If not stated otherwise, 6x bilayer have been built up followed by a 30 min incubation in phosphate buffer, pH 7 at 40 °C for film stabilization. Finally the DNA-electrodes were ready for measurements or have been stored dry at 4 °C in the dark. At all incubation stages cyclic voltammograms have been recorded to verify the assembly process.

Electrochemical experiments

Electrochemical measurements have been performed using the potentiostat CHI660E (CHI) and a custom-made electrochemical cell containing 1 mL of phosphate buffer (5 mM, pH 7) a Pt counter electrode and an Ag/AgCl (3 M KCl)

reference electrode. Cyclic voltammetric measurements have been performed at a scan rate of 100 mV s^{-1} and in a potential range from +300 to -300 mV.

Photoelectrochemical experiments

Photoelectrochemical measurements have been performed using an integrated system (CIMPS, Zahner) containing a white LED light source (4300 K, Zahner) with adjustable intensity (max. 100 mW cm^{-2}), an electrochemical cell and a photodiode with feedback control to the light source via a potentiostat (PP211, Zahner). Electrochemical investigations have been carried out through a coupled potentiostat (Zennium, Zahner). In all experiments a Pt counter electrode and an Ag/AgCl (3 M KCl) reference electrode have been used in an aqueous solution containing phosphate buffer (5 mM, pH 7). For most experiments no additional electron acceptor was used and air saturation of the solutions has been ensured. Photochronoamperometric experiments have been performed at RT and -100 mV vs. Ag/AgCl, while using an illumination time of 30 s and a light power of 20 mW cm^{-2} (white light source spectrum see Fig. S8). Light power dependent photocurrent experiments have been done using a power range of 0.5 – 20 mW cm^{-2} using white light with and without 1 mM of the soluble electron acceptor methyl viologen (MV^{2+}).

Surface plasmon resonance

Surface plasmon resonance (SPR) experiments have been performed on a Biacore T100 (GE Healthcare) at a constant flow rate of 1 µL min^{-1} and 25 °C. Before use, Au sensor chips have been cleaned with a low pressure air plasma. The clean Au surface has been incubated 48 h at RT with a freshly prepared ethanolic solution of a mixture containing MUA and MU. After the thorough washing of the surface with ethanol and phosphate buffer (5 mM, pH 7) the chip was ready to use. First cyt *c* has been adsorbed on the thiol layer forming the cyt *c* ML. PSI:cyt *c* pre-complex mixtures (1:20 and 1:100) have been flushed over the surface with different injection times.

Scanning electron microscopy

Au-chip-electrodes (Micrux) have been used and 6x bilayer of Au-cyt *c* ML-[PSI:cyt *c*] and Au-ML-DNA-[PSI:cyt *c*/DNA] have been prepared, according to the previously described procedure in this study. Functionality of the assembly has been verified via photochronoamperometric measurements. To elucidate profile heights of the assembly, electrode surfaces have been carefully cut with an ultrasharp blade in order to obtain sharp edges. For visualization of morphology of the prepared electrodes scanning electron microscopy (JSM-6510, JEOL) has been employed. The acceleration voltage was 5 kV, which allowed a non-destructive irradiation of the biological surface. A working distance of 20 mm and a magnification of 10,000 and 20,000 fold were chosen. Images have been recorded under an approximate angle of 85° relative to the surface normal.

Acknowledgements

Notes and references

1   A. Sassolas, L. J. Blum and B. D. Leca-Bouvier, *Biotechnol. Adv.*, 2012, **30**, 489–511.

2   N. Czechowski, H. Lokstein, D. Kowalska, K. Ashraf, R. J. Cogdell and S. Mackowski, *Appl. Phys. Lett.*, 2014, **105**, 043701.

3   X. Dominguez-Benetton, S. Srikanth, Y. Satyawali, K. Vanbroekhoven and D. Pant, *J. Microb. Biochem. Technol.*, 2013, **S6**, 007.

4   D. Leech, P. Kavanagh and W. Schuhmann, *Electrochim. Acta*, 2012, **84**, 223–234.

5   A. Badura, T. Kothe, W. Schuhmann and M. Rögner, *Energy Environ. Sci.*, 2011, **4**, 3263.

6   T. Kothe, N. Plumeré, A. Badura, M. M. Nowaczyk, D. a Guschin, M. Rögner and W. Schuhmann, *Angew. Chem. Int. Ed. Engl.*, 2013, **52**, 14233–6.

7   P. I. Gordiichuk, G.-J. A. H. Wetzelaer, D. Rimmerman, A. Gruszka, J. W. de Vries, M. Saller, D. A. Gautier, S. Catarci, D. Pesce, S. Richter, P. W. M. Blom and A. Herrmann, *Adv. Mater.*, 2014, **26**, 4863–4869.

8   A. Operamolla, R. Ragni, F. Milano, R. Roberto Tangorra, A. Antonucci, A. Agostiano, M. Trotta and G. Farinola, *J. Mater. Chem. C*, 2015, **3**, 6471–6478.

9   N. Plumeré, *Nat. Nanotechnol.*, 2012, **7**, 616–7.

10 F. Wang, X. Liu and I. Willner, *Adv. Mater.*, 2013, **25**, 349–77.

11 N. Nelson and C. F. Yocum, *Annu. Rev. Plant Biol.*, 2006, **57**, 521–65.

12 P. Jordan, P. Fromme, H. T. Witt, O. Klukas, W. Saenger and N. Krauss, *Nature*, 2001, **411**, 909–17.

13 A. Díaz-Quintana, W. Leibl, H. Bottin and P. Sétif, *Biochemistry*, 1998, **37**, 3429–39.

14 I. Grotjohann and P. Fromme, *Photosynth. Res.*, 2005, **85**, 51–72.

15 W. A. Cramer, H. Zhang, J. Yan, G. Kurisu and J. L. Smith, *Annu. Rev. Biochem.*, 2006, **75**, 769–90.

16 K. Nguyen and B. D. Bruce, *Biochim. Biophys. Acta*, 2014, **1837**, 1553–66.

17 B. S. Ko, B. Babcock, G. K. Jennings, S. G. Tilden, R. R. Peterson, D. Cliffel and E. Greenbaum, *Langmuir*, 2004, **20**, 4033–4038.

18 H. A. Kincaid, T. Niedringhaus, M. Ciobanu, D. E. Cliffel and G. K. Jennings, *Langmuir*, 2006, **22**, 8114–20.

19 I. Carmeli, L. Frolov, C. Carmeli and S. Richter, *J. Am. Chem. Soc.*, 2007, **129**, 12352–3.

20 M. Ciobanu, H. A. Kincaid, V. Lo, A. D. Dukes, G. Kane

Jennings and D. E. Cliffel, *J. Electroanal. Chem.*, 2007, **599**, 72–78.

21 X. Yan, C. J. Faulkner, G. K. Jennings and D. E. Cliffel, *Langmuir*, 2012, **28**, 15080–6.

22 A. K. Manocchi, D. R. Baker, S. S. Pendley, K. Nguyen, M. M. Hurley, B. D. Bruce, J. J. Sumner and C. a Lundgren, *Langmuir*, 2013, **29**, 2412–9.

23 N. Terasaki, N. Yamamoto, T. Hiraga, I. Sato, Y. Inoue and S. Yamada, *Thin Solid Films*, 2006, **499**, 153–156.

24 R. A. Grimme, C. E. Lubner, D. A. Bryant and J. H. Golbeck, *J. Am. Chem. Soc.*, 2008, **130**, 6308–9.

25 R. A. Grimme, C. E. Lubner and J. H. Golbeck, *Dalton Trans.*, 2009, 10106–13.

26 N. Terasaki, N. Yamamoto, T. Hiraga, Y. Yamanoi, T. Yonezawa, H. Nishihara, T. Ohmori, M. Sakai, M. Fujii, A. Tohri, M. Iwai, Y. Inoue, S. Yoneyama, M. Minakata and I. Enami, *Angew. Chem. Int. Ed. Engl.*, 2009, **48**, 1585–7.

27 O. Yehezkeli, O. I. Wilner, R. Tel-Vered, D. Roizman-Sade, R. Nechushtai and I. Willner, *J. Phys. Chem. B*, 2010, **114**, 14383–8.

28 A. Efrati, O. Yehezkeli, R. Tel-Vered, D. Michaeli, R. Nechushtai and I. Willner, *ACS Nano*, 2012, **6**, 9258–66.

29 S. C. Feifel, K. R. Stieger, H. Lokstein, H. Lux and F. Lisdat, *J. Mater. Chem. A*, 2015, **3**, 12188–12196.

30 V. B. Shah, W. R. Henson, T. S. Chadha, G. Lakin, H. Liu, R. E. Blankenship and P. Biswas, *Langmuir*, 2015, **31**, 1675–82.

31 K. R. Stieger, S. C. Feifel, H. Lokstein and F. Lisdat, *Phys. Chem. Chem. Phys.*, 2014, **16**, 15667–74.

32 A. Efrati, R. Tel-Vered, D. Michaeli, R. Nechushtai and I. Willner, *Energy Environ. Sci.*, 2013, **6**, 2950.

33 O. Yehezkeli, R. Tel-Vered, D. Michaeli, R. Nechushtai and I. Willner, *Small*, 2013, **9**, 1–9.

34 E. A. Gizzie, G. LeBlanc, G. K. Jennings and D. E. Cliffel, *ACS Appl. Mater. Interfaces*, 2015, **7**, 9328–35.

35 A. Badura, D. Guschin, T. Kothe, M. J. Kopczak, W. Schuhmann and M. Rögner, *Energy Environ. Sci.*, 2011, **4**, 2435.

36 F. Zhao, F. Conzuelo, V. Hartmann, H. Li, M. M. Nowaczyk, N. Plumeré, M. Rögner and W. Schuhmann, *J. Phys. Chem. B*, 2015, **119**, 13726–31.

37 T. Kothe, S. Pöller, F. Zhao, P. Fortgang, M. Rögner, W. Schuhmann and N. Plumeré, *Chemistry*, 2014, **20**, 11029–34.

38 V. Hartmann, T. Kothe, S. Pöller, E. El-Mohsnawy, M. M. Nowaczyk, N. Plumeré, W. Schuhmann and M. Rögner, *Phys. Chem. Chem. Phys.*, 2014, **16**, 11936–41.

39 D. R. Baker, R. F. Simmerman, J. J. Sumner, B. D. Bruce and C. A. Lundgren, *Langmuir*, 2014, **30**, 13650–5.

40 C. J. Faulkner, S. Lees, P. N. Ciesielski, D. E. Cliffel and G. K. Jennings, *Langmuir*, 2008, **24**, 8409–12.

41 G. LeBlanc, K. M. Winter, W. B. Crosby, G. K. Jennings and D. E. Cliffel, *Adv. Energy Mater.*, 2014, **4**, n/a–n/a.

Nanoscale Accepted Manuscript

42   E. Darby, G. LeBlanc, E. A. Gizzie, K. M. Winter, G. K.
      Jennings and D. E. Cliffel, *Langmuir*, 2014, **30**, 8990–4.

43   G. LeBlanc, G. Chen, E. a Gizzie, G. K. Jennings and D. E.
      Cliffel, *Adv. Mater.*, 2012, **24**, 5959–62.

44   P. N. Ciesielski, C. J. Faulkner, M. T. Irwin, J. M. Gregory, N.
      H. Tolk, D. E. Cliffel and G. K. Jennings, *Adv. Funct. Mater.*,
      2010, **20**, 4048–4054.

45   L. Frolov, O. Wilner, C. Carmeli and I. Carmeli, *Adv. Mater.*,
      2008, **20**, 263–266.

46   K. Ocakoglu and T. Krupnik, *Adv. Funct. Mater.*, 2014, **24**,
      7467–7477.

47   D. Sarauli, J. Tanne, D. Schäfer, I. W. Schubart and F. Lisdat,
      Electrochem. Commun., 2009, **11**, 2288–2291.

48   F. Wegerich, P. Turano, M. Allegrozzi, H. Möhwald and F.
      Lisdat, *Langmuir*, 2011, **27**, 4202–11.

49   C. Wettstein, H. Möhwald and F. Lisdat,
      Bioelectrochemistry, 2012, **88**, 97–102.

50   S. C. Feifel, A. Kapp, R. Ludwig, L. Gorton and F. Lisdat, *RSC
      Adv.*, 2013, **3**, 3428.

51   F. Lisdat, R. Dronov, H. Möhwald, F. W. Scheller and D. G.
      Kurth, *Chem. Commun. (Camb).*, 2009, 274–83.

52   M. K. Beissenhirtz, F. W. Scheller, W. F. M. Stöcklein, D. G.
      Kurth, H. Möhwald and F. Lisdat, *Angew. Chem. Int. Ed.
      Engl.*, 2004, **43**, 4357–60.

53   S. M. Bonk and F. Lisdat, *Biosens. Bioelectron.*, 2009, **25**,
      739–44.

54   S. C. Feifel and F. Lisdat, *J. Nanobiotechnology*, 2011, **9**, 59.

55   C. Wettstein, C. Kyne, A. M. Doolan, H. Möhwald, P. B.
      Crowley and F. Lisdat, *Nanoscale*, 2014, **6**, 13779–86.

56   H. Xie, D. Yang, A. Heller and Z. Gao, *Biophys. J.*, 2007, **92**,
      L70–2.

57   A. Nakamura, T. Suzawa, Y. Kato and T. Watanabe, *Plant
      Cell Physiol.*, 2011, **52**, 815–23.

58   P. R. Chitnis, *Annu. Rev. Plant Physiol. Plant Mol. Biol.*,
      2001, **52**, 593–626.

59   E. Y. Katz, Y. N. Kozlov and B. A. Kiselev, *Energy Convers.*,
      1979, **19**, 73–75.

60   T. Fujii, E. Yokoyama, K. Inoue and H. Sakurai, *Biochim.
      Biophys. Acta - Bioenerg.*, 1990, **1015**, 41–48.

61   T. Bennett, H. Niroomand, R. Pamu, I. Ivanov, D. Mukherjee
      and B. Khomami, *Phys. Chem. Chem. Phys.*, 2016, **18**, 8512–
      21.

62   K. Brettel and W. Leibl, *Biochim. Biophys. Acta*, 2001, **1507**,
      100–14.

63   V. Proux-Delrouyre, C. Demaille, W. Leibl, P. Sétif, H. Bottin
      and C. Bourdillon, *J. Am. Chem. Soc.*, 2003, **125**, 13686–92.

64   J. Kern, B. Loll, C. Lüneberg, D. DiFiore, J. Biesiadka, K.-D.
      Irrgang and A. Zouni, *Biochim. Biophys. Acta*, 2005, **1706**,
      147–57.

65   B. Ge and F. Lisdat, *Anal. Chim. Acta*, 2002, **454**, 53–64.